

Review

An EEG Finger-Print of fMRI deep regional activation

Yehudit Meir-Hasson ^{a,*}, Sivan Kinreich ^b, Ilana Podlipsky ^b, Talma Hendler ^{b,c,d,e}, Nathan Intrator ^{a,c}^a The Blavatnik School of Computer Science, Tel-Aviv University, Tel-Aviv, Israel^b Functional Brain Center, Wohl Institute for Advanced Imaging, Tel-Aviv Sourasky Medical Center, Israel^c Sagol School of Neuroscience, Tel-Aviv University, Tel-Aviv, Israel^d School of Psychological Sciences, Tel-Aviv University, Tel-Aviv, Israel^e Sackler Faculty of Medicine, Tel-Aviv University, Tel-Aviv, Israel

ARTICLE INFO

Article history:

Accepted 4 November 2013

Available online xxxx

Keywords:

Simultaneous fMRI/EEG

EEG Finger-Print

Time/frequency

Ridge-regression

ABSTRACT

This work introduces a general framework for producing an EEG Finger-Print (EFP) which can be used to predict specific brain activity as measured by fMRI at a given deep region. This new approach allows for improved EEG spatial resolution based on simultaneous fMRI activity measurements. Advanced signal processing and machine learning methods were applied on EEG data acquired simultaneously with fMRI during relaxation training guided by on-line continuous feedback on changing alpha/theta EEG measure. We focused on demonstrating improved EEG prediction of activation in sub-cortical regions such as the amygdala. Our analysis shows that a ridge regression model that is based on time/frequency representation of EEG data from a single electrode, can predict the amygdala related activity significantly better than a traditional theta/alpha activity sampled from the best electrode and about 1/3 of the times, significantly better than a linear combination of frequencies with a pre-defined delay. The far-reaching goal of our approach is to be able to reduce the need for fMRI scanning for probing specific sub-cortical regions such as the amygdala as the basis for brain-training procedures. On the other hand, activity in those regions can be characterized with higher temporal resolution than is obtained by fMRI alone thus revealing additional information about their processing mode.

© 2013 Elsevier Inc. All rights reserved.

Contents

Introduction	0
Methods	0
Experiment setup and pre-processing	0
Post-processing	0
The prediction model	0
Results	0
Prediction of the visual cortex	0
Prediction of subcortical/limbic activity	0
Discussion	0
Acknowledgments	0
Appendix A. Supplementary data	0
References	0

Introduction

Modulating deep brain activity (Harris-Warrick and Marder, 1991) is necessary to improve mechanism driven therapeutic approaches in patients with neurological and psychiatric disorders such as schizophrenia (Haraldsson et al., 2004), post traumatic stress disorder (PTSD)

(Novakovic et al., 2011), Tourette's syndrome (Ackermans et al., 2008), and Parkinson's disease (Honey and Ranjan, 2012). In this regard, recent efforts have been done to focus on the use of brain imaging knowledge on specific neural circuits to guide deep brain stimulation and neuro-feedback procedures (See recent reviews (Pandurangi et al., 2012; Horowitz, 2012) respectively).

A necessary condition for such integration is the ability to detect brain activity in deep regions related to various disorders. Ostensibly, EEG is an excellent method for marking neural processes due to its high temporal resolution on the order of milliseconds. In addition, it is

* Corresponding author.

E-mail address: yehudit.hasson@gmail.com (Y. Meir-Hasson).

based on using a portable relatively low cost machine, thus enables high dissemination.

However, EEG has a significant disadvantage in term of localization since the estimation of sources of electrical activity from measurements on the skull is an ill-posed inverse problem (Baillet et al., 2001). This issue is further exacerbated by lack of information regarding individual geometry and inhomogeneous tissue conductivity (Gençer and Acar, 2004), and the limited number of recording channels. The localization limitation is especially severe with regard to the possibility to record activity originated at sub-cortical regions such as the hippocampus, amygdala and basal ganglia. These areas are highly relevant to a variety of neurological and psychiatric states since they are involved in major control mechanism of behavior including memory (Squire, 1992), emotion (LeDoux, 1992) and movement (Mink, 1996), respectively.

To estimate the brain activity in deep regions, additional sources should be integrated with EEG. In the last decade the use of simultaneous EEG/fMRI recording has become more common and received recognition as a reliable multi-modal measurement of brain activity. The main promise of such concurrent recording is that it may represent specific mental states with increased overall spatio-temporal resolution.

However, EEG and fMRI integration also has disadvantages; the fMRI is not a portable machine, its recording is expansive and the experience for the participant is not convenient due to the noise and discomfort lying inside the magnet. The EEG concurrent recording data on the other hand is much noisier than when recorded alone due to artifacts that emerge in a strong magnetic field. In addition, the integration of EEG with fMRI is not trivial; the two modalities are essentially different from a neural perspective. The EEG provides a direct measurement of the neuronal event and records the electrical potential changes in the cerebral cortex. The fMRI, on the other hand, provides an indirect measurement of the neural activity since increasing in the neuronal activity corresponds to increased oxygen demand and local cerebral blood flow (CBF). Hence the time frame of EEG and fMRI is completely different; while EEG corresponds to the immediate synchronized neural response, fMRI corresponds to the change in blood oxygen level-dependent (BOLD) signal following a pattern known as the hemodynamic response function (HRF), which typically peaks 4–6 s following the appearance of a neural event (Friston et al., 1994).

To overcome the above limitation while combining the advantages of each method we suggest using EEG to simulate the fMRI. Specifically, we want to find EEG features that can predict specific brain activity as measured simultaneously by the fMRI. We call that cluster of features an EEG Finger-Print (EFP). We hope that this new approach will reduce the need for fMRI scanning when analyzing sub-cortical regions and allow for using only the widely available EEG for real-time training. A cheaper portable machine which can represent deep brain activity may be useful for personal brain modulation operations performed on a daily basis for patients in neurology and psychiatry.

To begin with, we chose the amygdala as an example for a deep sub-cortical region which can be observed using the EEG. The amygdala is a core node in the limbic network which mediates the emotional processing in the brain by supporting functions like motivation, long-term memory, and affective tagging (LeDoux, 1992, 2000). We assume that any substantial activation in the limbic system will be reflected also in the amygdala. We focus on the amygdala since it has been shown to play a major role in the biased processing of negative stimuli and in the recognition of their aversive valence (Adolphs et al., 1995; Zald, 2003), as well as for an integrative stress response (Lang et al., 2000). In addition, activation of the amygdala has been related to difficulties in moderating the reaction to emotional stimuli in PTSD (Rauch et al., 2006). An fMRI study showed that PTSD patients exhibited exaggerated amygdala responses and diminished medial prefrontal cortex (mPFC) responses to fearful facial expressions (Shin et al., 2005). Moreover, mPFC activation was negatively correlated both with activation in the amygdala and with symptom severity post exposure to military stress, as shown in a prospective fMRI study by our lab (Admon et al., 2009).

Thus, having an easy to use method for training self-modulation of the amygdala's response seems like a promising tool for effective coping with stressful situations.

We suggest finding EEG features (i.e. which we term EEG Finger-Print) that can predict specific brain activity, which is indicated by simultaneous fMRI recording, by integrating information taken from the fMRI. In the past, mainly two approaches for integration of EEG and fMRI have been suggested (for review, see Huster et al., 2012; Rosa et al., 2010); the first, treats the EEG and the fMRI data symmetrically entailing a single fusion model that can explain both the EEG and fMRI data (Valdes-Sosa et al., 2009). The second applies an asymmetric approach by analyzing one modality using some reliable information taken from the other modality (de Munck et al., 2007; Goldman et al., 2002; Liu et al., 1998).

The symmetric approach tried originally to construct a common forward/generative model that maps from neuronal activity to both hemodynamic and electromagnetic measurement (Valdes-Sosa et al., 2009). In practice, constructing the neurophysiologic model from the EEG/fMRI data is difficult due to lack of precise knowledge regarding the neural mechanisms. Instead, more current symmetric models try to find a common substrate that may explain some features in both EEG and fMRI measurements (Daunizeau et al., 2007; Deneux and Faugeras, 2010; Luessi et al., 2011). Other symmetric data-driven fusion methods explore the associations between some features in the EEG and some features in the fMRI without an a priori bias of either. Examples are: measuring the mutual dependence between the two modalities after decomposition into components (Correa et al., 2010; Martinez-Montes et al., 2004), reducing each of the modality into a feature space and examining the relationships between them using joint ICA (Calhoun and Adali, 2009; Moosmann et al., 2008) or maximizing the correlation after applying transfer functions on each of the modalities (Bießmann et al., 2010).

The asymmetric approach can be applied in either direction; one direction tries to improve EEG with respect to localization based on fMRI BOLD signal constraints. Typically, improving EEG spatial localization was viewed as an ill-posed source localization problem without a unique inverse solution. The inverse problem solution depends on the EEG modeling; whether a fixed number of dipoles are assumed a priori or not (i.e. equivalent current dipole model vs. the distributed source model, for review, see Grech et al., 2008). In both cases, anatomical and functional constraints from the fMRI can be used to constrain the location of the activity (Ahlfors et al., 1999; Dale et al., 2000; Korvenoja et al., 1999; Liu et al., 1998; Phillips et al., 2002). Different regularization techniques were suggested to solve the inverse problem such as Wiener filter (Dale et al., 2000; Liu et al., 1998), weighted minimum norm (Ahlfors and Simpson, 2004; Babiloni et al., 2005), Bayesian method (Henson et al., 2010; Mattout et al., 2006; Phillips et al., 2005; Sato et al., 2004) and Twomey regularization (Liu et al., 2006). Other "time-variant" spatial constraints to address the EEG source localization problem came by fusing data from both fMRI and EEG (Brookings et al., 2009; Liu and He, 2008). Another study estimated the model parameters for each region independently to reduce the constraint imposing similarity of the activation time-courses across regions (Ou et al., 2010).

The second asymmetric approach uses EEG to analyze the fMRI BOLD signals; searching in the fMRI data areas which are in correlation with temporal information in the EEG. For this purpose, an EEG predictor is built based on prior knowledge or EEG analysis. The EEG predictor is convolved with the standard hemodynamic response function (HRF) (Friston et al., 1994) and its temporal resolution is reduced to the fMRI temporal resolution. Then, the processed EEG predictor is used as a regressor in a standard voxel-wise GLM analysis. Several approaches for computing EEG predictor exist; taking the average spectrogram in intervals of interest (Ben-Simon et al., 2008; Goldman et al., 2002; Goncalves et al., 2006; Laufs et al., 2003a,b; Moosmann et al., 2003), using the amplitude modulations of single trial ERPs (Eichele et al., 2005) and applying the previous methods following decomposition into components

such as PCA, and ICA (Debener et al., 2005). De Martino et al. (2010) used prediction instead of GLM and estimated the fMRI patterns associated with a processed EEG signal using Relevance Vector Machine (RVM) and Ridge Regression (RR).

Recent studies tried to improve EEG interpretation of a specific phenomenon, such as activity at a certain region using the BOLD signal from this area as a constraint. De-Munck et al. showed that a data-driven estimation of the hemodynamic response shape of the alpha power in specific voxel can improve the prediction of the BOLD signal taken from this voxel (de Munck et al., 2007). Later research estimated the hemodynamic response shape for other frequency bands (each one separately) (de Munck et al., 2009). Another event related study showed that linear regression including all frequency bands predicted BOLD better than individual frequency band (performed in MEG after averaging over trials and convolution with subject-specific HRF, uniform for all frequencies) (Zumer et al., 2010).

Extending the above recent studies, we suggest a general framework to improve EEG interpretation/prediction of fMRI brain activity of a specific region in a single trial level using the BOLD signal from the region of interest as a constraint. Our approach tries to overcome four main limitations of the traditional approach: first, we do not assume a pre-defined delay between the modalities, which uses a fixed HRF and ignores intra-variability between subjects and inter-variability between regions and frequencies (Aguirre et al., 1998). Rather, we suggest using a specific data-driven time-delay for each subject, electrode and frequency. Second, we do not drastically reduce the temporal resolution of the EEG, which may ignore important temporal information stored in the EEG. Rather, we sub-sample at the time/frequency representation, rather than the raw signal (De Martino et al., 2010). In this way, while we sample at low frequency, we still get information about activity in high frequencies (Stockwell, 2007). Furthermore, we suggest to increase slightly the temporal resolution of the BOLD signal (to improve the matching between the signals). Third, instead of choosing the relevant electrodes and frequencies based on prior knowledge or prior EEG analysis, we introduce a data-driven approach to find the most relevant electrodes and frequencies which best contribute to the fMRI ROI prediction. The tradeoff of this limitation is pre-selection of the fMRI ROI. Fourth, as the use of GLM/correlation may be sensitive to overfitting, we suggest to use a machine learning approach with robust statistic methods including regularization and cross-validation, for model selection and validation (Hasson-Meir et al., 2011; Podlipsky et al., 2012). We demonstrate that the proposed set of solutions constructs a robust model, which better predicts an unseen fMRI BOLD signal.

We demonstrate the ability of the suggested framework to find an EEG Finger-Print (i.e. EEG features) that can predict the fMRI BOLD activity in the amygdala during real-time relaxation training guided by alpha/theta neurofeedback. In particular, we show that a ridge regression model, which is based on time/frequency representation of EEG data from a single electrode where each frequency band has its own delay, can predict the amygdala activity better than a linear combination of frequencies with a pre-defined delay and significantly better

than traditional theta/alpha activity. Our ultimate goal is to build a robust EEG model, using the fMRI measurements as gold-standard, and to be able to reduce the need for fMRI scanning for probing specific sub-cortical regions.

Methods

This section introduces the proposed approach to build an EEG Finger-Print of fMRI ROI. Fig. 1 demonstrates the flowchart of the EFP method. It contains the following steps: 1) preprocessing to remove artifacts from the raw data. 2) Selecting electrodes of interest in the EEG and ROI in the fMRI 3) Post processing operations which construct the response variable in the fMRI and the feature space in the EEG (i.e. transformation into time-frequency domain, averaging into bands and considering different time delays) 4) Prediction of the processed fMRI ROI using processed EEG data. Prediction results give a feedback on the activated electrodes, frequencies and time-delays.

The initial preprocessing is aimed at removing artifacts related to data acquisition. These have to do with movement (cardio-ballistic and other) during acquisition and are exacerbated when using EEG electrodes inside a large magnetic field (see further in section "Experiment setup and pre-processing", where each data set has its own adjustments). Then, a region of interest in the fMRI is extracted and interesting electrodes in the EEG are selected. We can choose to work with several electrodes which are known to be activated when the specific region is activated, or take all the electrodes and let the algorithm find the most relevant electrodes.

Experiment setup and pre-processing

The proposed framework is generic and can be applied to any EEG-fMRI simultaneous recording. Here, we demonstrate the performance of the framework on the following two experiments.

In the first experiment, four subjects were requested to open and close their eyes in a lighted room every 30 s for 3 min (see Ben-Simon et al., 2008 and method section for additional details). The EEG and the fMRI were recorded simultaneously. Pre-processing of the fMRI data using SPM included removing the first 20 s to allow steady state magnetization, realigning to the first scan, normalization into standard MNI space, spatial smoothing using a Gaussian kernel (FWHM = 4 mm) and high-pass filtered at 1/128 s. Pre-processing of the EEG data includes MR gradient artifacts and Cardio-ballistic artifacts removal and down sampling to 250 Hz.

For the construction of an alpha predictor, the EEG signals were averaged over the alpha band and over the relevant electrodes (the alpha range and the relevant electrodes were selected individually for each subject). The averaged signal was convolved with the canonical hemodynamic response function implemented in SPM. Additional information about the alpha predictor creation can be found in Ben-Simon et al. (2008). The four subjects that were selected from the original group of subjects described in Ben-Simon et al. (2008), had the highest

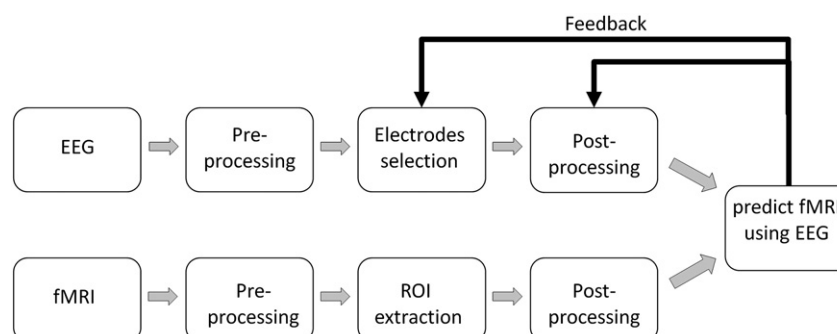


Fig. 1. Flowchart of the EFP method. Note the feedback which comes from prediction performance (on validation data) on the electrodes' selection and the post processing.

correlation between the alpha predictor and the target ROI. These subjects, with a high SNR, were selected for proof of principle.

The second experiment, which is described in detail in Kinreich et al. (2011b) is based on previous studies showing that participants can be trained, relatively in a short time, to modulate their EEG waves (e.g. minutes) (Egner et al., 2002), included two stages; the first stage was training: EEG-NF (EEG-Neuro-Feedback) outside the fMRI. Subjects were asked to relax with eyes closed for 15 min. Changes in their theta/alpha activity were delivered back to the subjects as a soft tune (relaxed piano tune) via headphone. The feedback criterion was based on a scale of 10 possible values of T/A power ranging from 0.2 to 2 with 10% increase between every two sequential values. Each of these sequential increases corresponded to a specific sound intensity increasing or decreasing inversely proportional to T/A power. Real time theta (4–7 Hz) and alpha (8–13 Hz) signals were extracted from three occipital electrodes (Oz, O1, O2) (Peniston and Kulkosky, 1991) and averaged every 3 s, to calculate the ratio.

The second stage includes EEG-NF inside the fMRI scanner. Subjects followed a similar procedure to the EEG-NF protocol as during the training session twice for 15 min. Three individualized neuro-feedback electrodes were selected out of eight occipital electrodes (OZ, O1, O2, P3, PZ, P4, CP1, CP2) and used to extract the relevant EEG power for feedback. The chosen electrodes have the highest T/A amplitude during the training session. Twenty subjects participated in the experiment; each subject had two sessions except one subject which had one session (in total 39 sessions).

Pre-processing of the fMRI data using Brain-voyager (Brain Innovation, Maastricht, The Netherlands) included removing the 6 first seconds to allow steady state magnetization, slice timing correction, motion correction, normalization into Talairach space, and spatial smoothing using a Gaussian kernel (3-mm FWHM). Pre-processing of the EEG data includes MR gradient artifacts and Cardio-ballistic artifacts removal and down sampling to 250 Hz.

For the construction of a T/A predictor, theta (4–7 Hz) and alpha (8–12 Hz) signals were extracted from a single electrode and their ratio was convolved with the canonical hemodynamic response function implemented in SPM. The electrode whose T/A achieved the highest correlation with the target ROI was chosen. The 'best' session of each subject (the one with the highest T/A prediction result) was chosen for further analysis ($n = 20$).

Post-processing

The post-processing operations construct the response variable in the fMRI and the feature space in the EEG (see Fig. 2).

Following the extraction of a region of interest in the fMRI, the BOLD signal is up-sampled to 4 Hz using cubic-spline interpolation and normalized to have a zero mean and one standard deviation.

The multi-dimensional EEG time series is converted into a time/frequency representation using Stockwell-transformation (ST) (Stockwell et al., 1996). The transform frequency resolution was set to 1 Hz with temporal resolution of 250 Hz, which is the original sampling rate of the EEG. ST is similar to the STFT (Short-time Fourier transform) except that the width of the window is frequency-dependent, becoming narrower at higher frequencies. An example of the application of the ST to EEG recordings appears in Podlipsky et al. (2012).

The converted EEG signals are down-sampled to 4 Hz and the frequency resolution is reduced by splitting into 10 frequency bands, which are defined using an energy uniformity constraint on the EEG data, and averaging the energy over each band. Those bands divide the spectral logarithmic mean of the original EEG (before ST transformation) into 10 equal areas. This division is similar to the approach applied in vision (Atick and Redlich, 1992). After dividing into bands, the EEG data is normalized for easier interpretability of prediction weights (each frequency band has a zero mean).

Since the HRF is known to have inter-variability between electrodes and frequencies and intra-variability between subjects (Aguirre et al., 1998), continuous time delay between the EEG and the fMRI is considered. Our features space is defined as following:

$$[\text{CH}] \times [\text{FQ}] \times [\text{DELAY}] \times [\text{TIME}] \quad (1)$$

Activity which can be seen in the fMRI in time T can be predicted in the EEG using the intensity of frequency FQ of electrode CH in delay D from T.

The prediction model

Improvement of EEG interpretation of activity from a certain brain region using the BOLD signal taken from this region is achieved by finding the electrodes, frequencies and delays (i.e. an EEG Finger-Print) which contribute to activation in the ROI BOLD signal. This EEG Finger-Print can be used to predict the ROI fMRI signal. For this purpose, for each electrode a family of models is constructed, with different combinations of frequency bands, time delays and model constraints. Each member of the family attempts to predict the ROI signal by finding the coefficients of the model, which best describes the activity in this ROI. A smaller collection of "optimal" models is selected from the above large family of models, using classical robust statistics methods for model selection and validation. Each model in the "optimal models" set represents the best finger-print found for unique electrode. The model, which best predicts the ROI activity, suggests the most informative electrode and provides interpretation of the model; the coefficients suggest frequency bands and time delays, which correlated to the ROI activity (i.e. finger-print).

We used a family of regularized Ridge Regression (RR) models to predict the fMRI BOLD signal. The regularized model can be used with a variety of linear and nonlinear regressors. Since the exact relationship between the two integrated signals is unclear; RR is a good starting point as it is also optimal in terms of simplicity, interpretability of its coefficients and speed. Given the independent variable X (i.e. the EEG processed data) and the dependent variable y (i.e. the fMRI BOLD signal), RR seeks w which minimizes the following equation:

$$\|y - Xw\|^2. \quad (2)$$

A regularization term λ (Tikhonov, 1963) is added to the least-squares equation to control the potential singularity of the associated covariance matrix (Hoerl and Kennard, 1970). This λ imposes a penalty on large fluctuations of the estimated parameter w and respectively on the fitted function.

$$\|y - Xw\|^2 + \lambda \|w\|^2 \quad (3)$$

The fact that the EFP method allows a sliding delay increases the model's number of parameters and hence it is likely that the model found would fit better to the data up to over-fitting (Occam's razor principle). The over-fitting problem is handled in this paper by using classical robust statistic methods for model selection and validation. These include cross validation and regularization at several levels of the feature extraction (Hasson-Meir et al., 2011; Podlipsky et al., 2012). Regularization reduces over-fitting by penalizing weight parameters (see Inline Supplementary Fig. S1). In cross-validation, the data is divided into several disjoint training and testing sets. This is used to avoid over-fitting which results from the large number of free parameters with respect to the size of the training data (Efron and Tibshirani, 1993).

Inline Supplementary Fig. S1 can be found online at <http://dx.doi.org/10.1016/j.neuroimage.2013.11.004>.

The cross-validation is applied twice (see Inline Supplementary Fig. S2); first for dividing the original data into train and test sets. We search for the optimal models (for each electrode, the model which

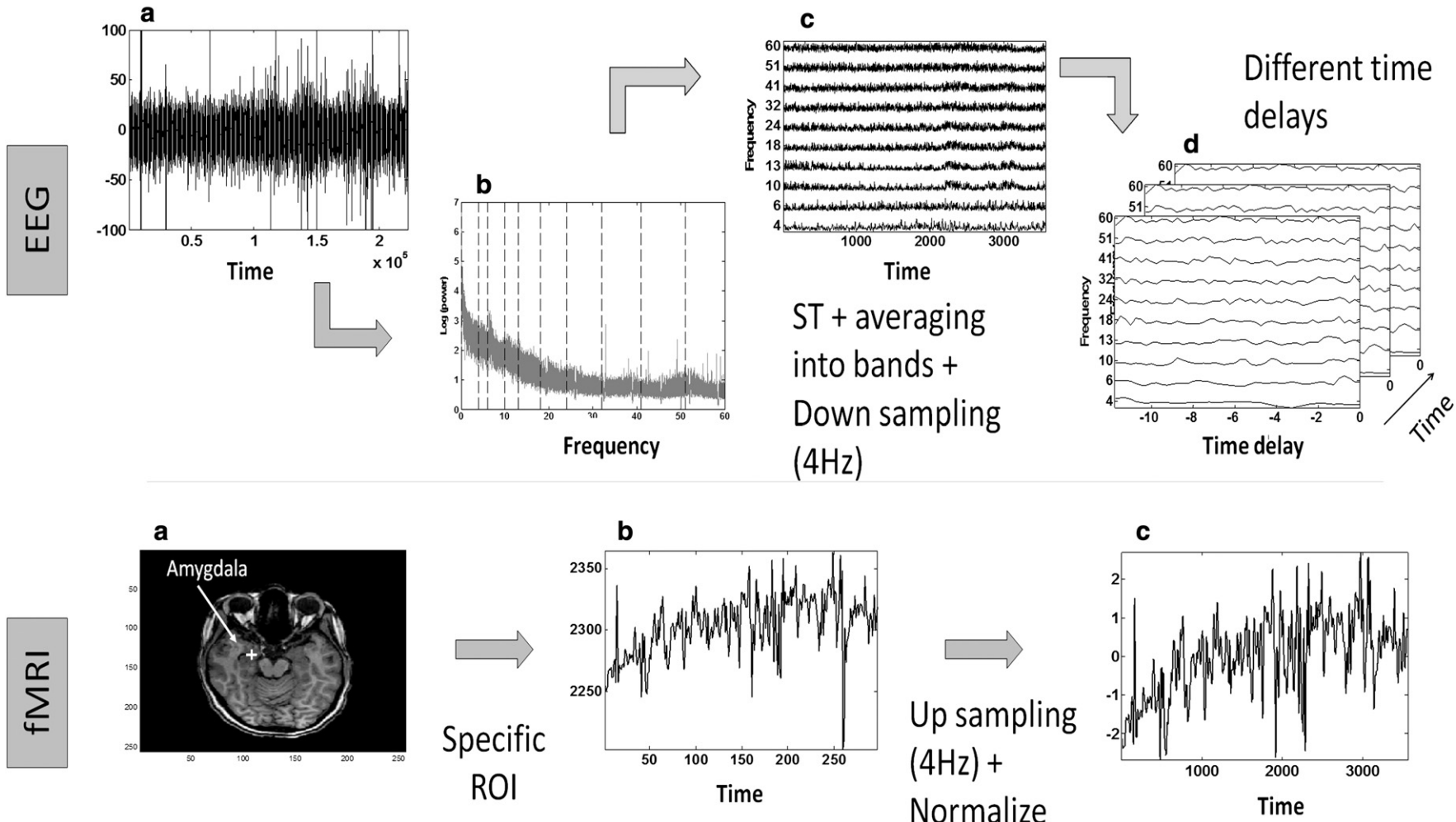


Fig. 2. Details of the post-processing stage. In the EEG, each electrode (a) is converted into time-frequency representation and reduced to 4 Hz. Data-driven bands are selected (b) and the time-frequency matrix (which originally has frequency resolution of 1 Hz) is averaged over those bands (c). A window of time in the EEG is considered for each time-point in the fMRI (d). In the fMRI, the extracted ROI (b) is up-sampled to 4 Hz and normalized (c).

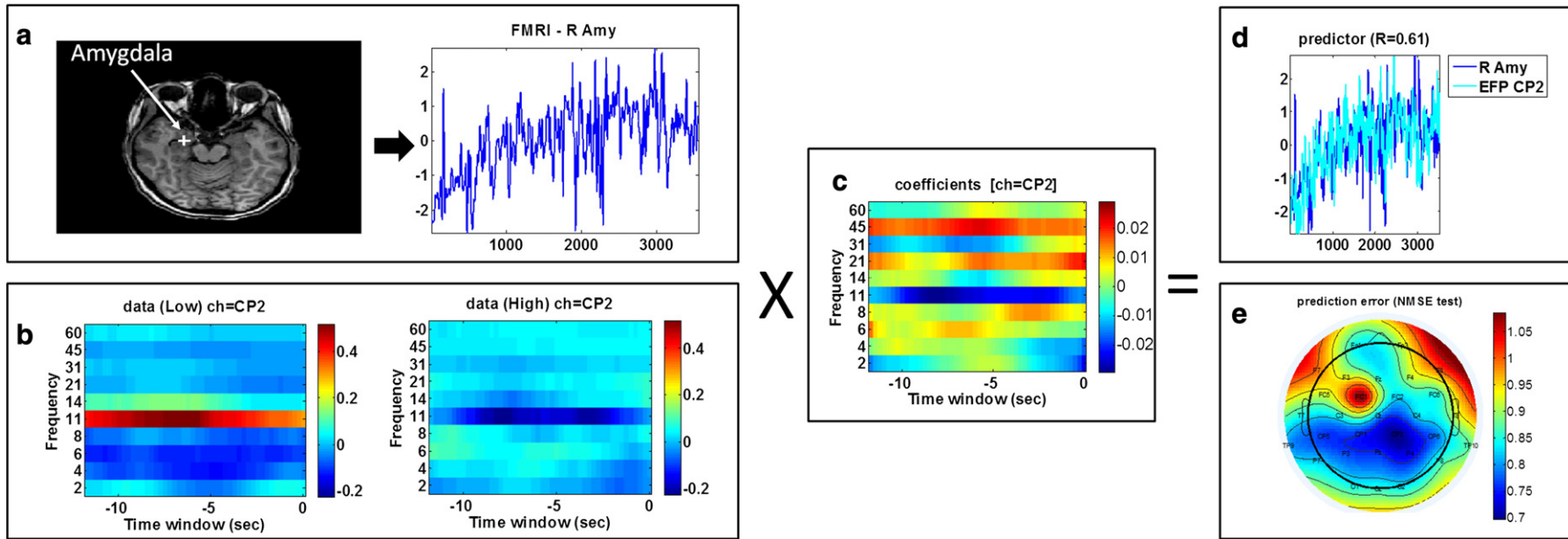


Fig. 3. Prediction input and output. a) Processed ROI signal and b) processed EEG data of a specific electrode. Two matrices are demonstrated. The left one is an average matrix of the entire EEG data related to lower 25% values of the ROI signal and the right one is an average matrix of the entire EEG data related to upper 25% values of the ROI. c) The EFP derived by the prediction model. Increased activity in the fMRI signal can be indicated by strong red coefficients which relate to increased activity in that time-frequency range or strong blue coefficients which relate to decreased activity in that time-frequency range. d) The predictor generated using the coefficients found. This predictor contains the same information as the ROI signal but it was produced using EEG, so it is sensitive to changes in the EEG that occur in higher temporal resolution than the original fMRI signal. e) Map of the prediction error using each one of the electrodes. This map indicates which electrodes were more useful in the prediction of the specific ROI.

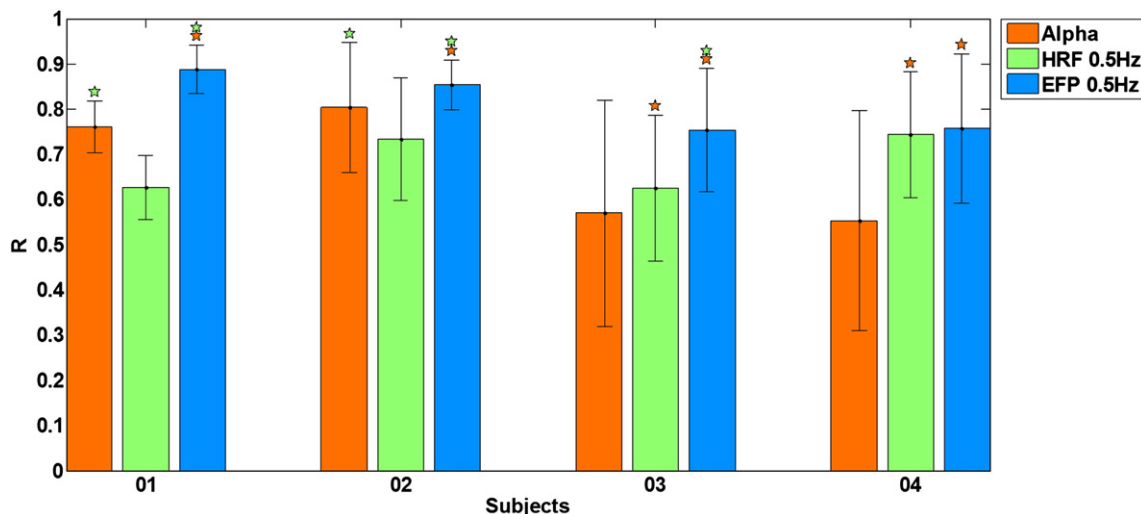


Fig. 4. Performance comparison between the alpha predictor, HRF and EFP predictors. Results indicate significant improvement of the EFP predictor compared to the Alpha predictor, in all subjects. EFP prediction improvement was obtained with respect to the HRF predictor in all of the subjects (75% of them were significant). The star's color represents the method that obtained significance ($*p < 0.05$). The subjects are ordered by an increasing p-value. The error bars are standard deviations over the cross-validation mk-folds. All methods were tested on the same train-test division.

best predicts the ROI activity) on the train sets and check their accuracy on the test sets. Second, an additional inner cross-validation procedure is applied for selecting the optimal models (i.e. finding the best regularization parameter) on the train sets.

Inline Supplementary Fig. S2 can be found online at <http://dx.doi.org/10.1016/j.neuroimage.2013.11.004>.

In the first $m \cdot k$ -fold cross validation, the original data is partitioned into k disjoint sets. To capture the variability of the continuous signal, each test set contains different sample blocks of the signal over time. A single dataset is retained as the test data for testing the models and

the remaining $k - 1$ disjoint sets are used as training data for choosing optimal models. We repeat this process m times, to have in total mk divisions into train and test sets. The cross-validation process is then repeated mk times, with each of the mk sets used exactly once as the test data ($k = 5$ and $m = 2$ are typically values chosen for good performance). The same $m \cdot k$ -fold cross-validation was used in all the methods, for a fair comparison, which also used the same train-test division.

The second n -fold cross-validation operation is used for finding the best regularization parameter; the training dataset is randomly split

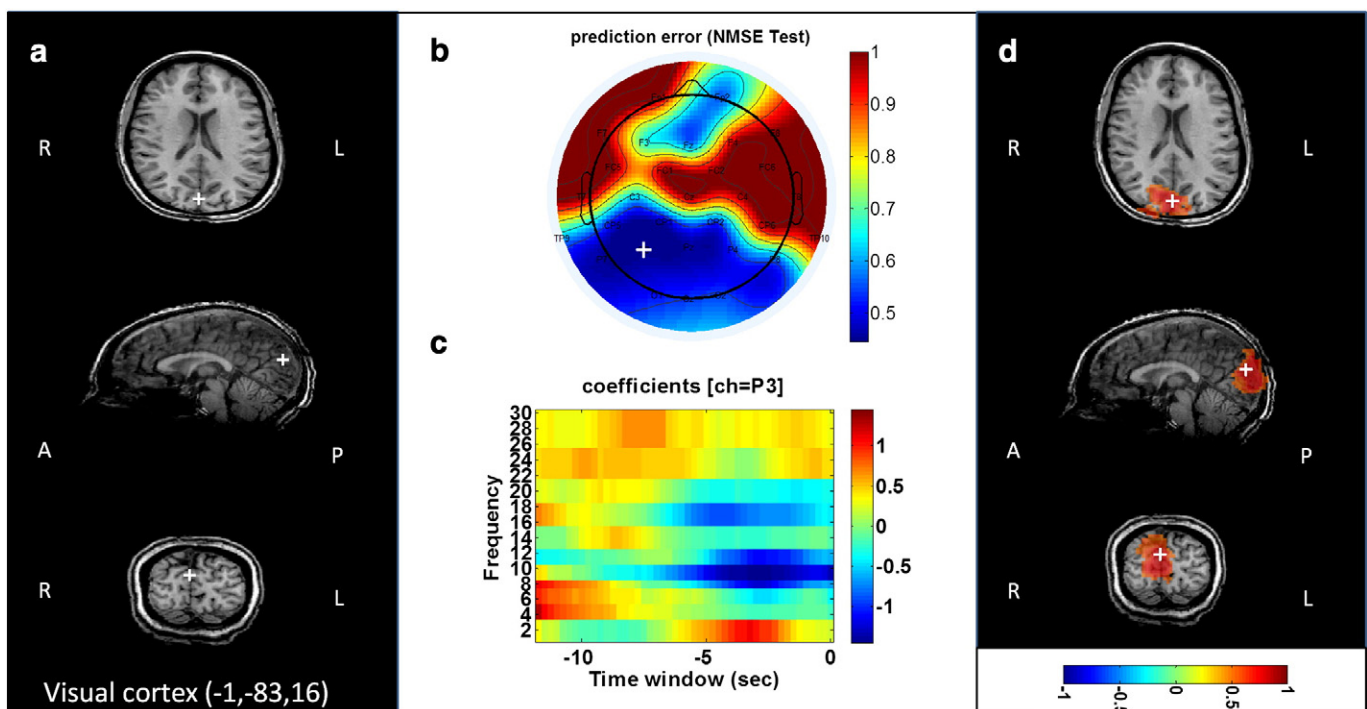


Fig. 5. The EFP for the visual cortex. a) The target ROI extracted from the visual cortex (Talairach $[-1, -83, 16]$, MNI $[-1, -86, 13]$, Gaussian sphere radius 6 mm). b) Averaged prediction error (NMSE) on test data for each electrode for all the subjects ($n = 4$, $p < 0.05$, FDR corrected). It is evident that the occipital electrodes produced minimal NMSE (marked as blue) i.e. best describe the activity in the visual cortex including our target ROI. c) Averaged EFP for electrode P3 for all the subjects ($n = 4$, $p < 0.05$, FDR corrected). It can be seen that the alpha band was modulated during the experiment and the best predicted delay between the modalities was around 3 s. d) Slices of the same section as in 5a, obtained from the whole brain parametric maps for all subjects show the distribution of activated voxels that are strongly predicted by the P3 EEG Finger-Print ($|R| >= 0.5$, $p < 0.05$, FDR corrected). The bottom bar shows the Pearson correlation value between signal intensity and EFP predictor.

(in block design), n times ($n = 30$), into 80–20% training and validation sets respectively. The regressor runs on the training set with different values of regularization parameter (within range of interest) and selects the one that yields the best results (i.e. bring normalized mean square error, NMSE, to minimum). The inner n -fold cross-validation was used both in the EFP method and the HRF method, which used a pre-defined delay, to discover optimal models subject to their respective free parameters.

The range of regularization parameters is determined using the singular values, which are obtained from SVD decomposition of the processed data matrix (used for training and testing). The range is bounded between the minimal and the squared maximal singular values. For computational efficiency, the actual regularization values in that range are distributed uniformly on the logarithmic scale.

Normalized mean squared error (NMSE) is used as a similarity measure between the fMRI signal and the predictor. If the NMSE is less than 1, then the prediction is doing better than the series mean.

$$\text{NMSE} = \text{MSE}(x)/\text{VAR}(x) = \sum_{i=1}^n (x_i - y_i)^2 / \sum_{i=1}^n (x_i - \bar{x})^2 \quad (4)$$

Another similarly measure used in this paper is the Pearson's correlation measure. It is useful for comparing the performance of our predictor and other EEG predictors which are known to have correlation with the BOLD activity in the investigated region. It should be noted that high correlation does not ensure exact similarity but only similar behavior. Pearson's correlation is given by:

$$\rho_{xy} = \text{corr}(X, Y) = E[(X - \bar{X})(Y - \bar{Y})] / (\sigma_x \sigma_y). \quad (5)$$

The correction for multiple comparisons was made with the false discovery rate (FDR) procedure (Storey, 2002). This procedure computes a p-value threshold that set the expected rate of falsely rejected null hypotheses to 5%. This procedure was used both for finding the electrodes that significantly predict the fMRI BOLD signal and the coefficients that significantly contribute to the prediction; The prediction

result of electrodes with non-significant prediction (after FDR correction) was set to zero/one (correlation/NMSE respectively). In a similar way, coefficients whose weight, are not FDR significantly different from zero were set to zero. Moreover, after constructing the predictor using the EFP method, FDR correction was used to set to zero voxels which are not significantly correlated with the predictor.

Fig. 3 shows the prediction input and output. Given a processed ROI signal and processed EEG data of a specific electrode, the prediction model finds the optimal model with coefficients that mostly describe the activity in the ROI. Those coefficients indicate relevant frequencies and time delay of the activity (i.e. an EEG Finger-Print). The predictor is sensitive to changes in the EEG that occur in higher temporal resolution than the original fMRI signal. The accuracy of the generated predictor is tested on the test sets. The smaller the prediction error, the prediction is better. Map of the prediction results on the test sets for each of the electrodes may indicate the activated areas during the mental process.

Results

Prediction of the visual cortex

We first applied the suggested method on an experiment which is known to produce a clear modulation of the alpha rhythm during rest; Hans Berger in 1929 found that the alpha power increases during eyes closed and decreases with eyes open (i.e. the "Berger effect"). Ben-Simon et al. (2008) used the eyes closed-eyes opened alpha modulation as a predictor for simultaneously recorded BOLD activation. Their analysis showed that activation confined as expected to the visual cortex and the thalamus were in correspondence to eyes closed while spontaneous alpha modulations were correlated with activation in medial wall regions such as medial prefrontal cortex and posterior cingulated cortex.

As proof of concept, we have used the data from this study obtained from 4 subjects (see Ben-Simon et al., 2008 and method section for additional details) and focused on an ROI extracted from the visual cortex (Talarach [-1, -83, 16], MNI [-1, -86, 13], Gaussian sphere radius 6 mm). The coordinates were chosen from the primary visual cortex area (V1)

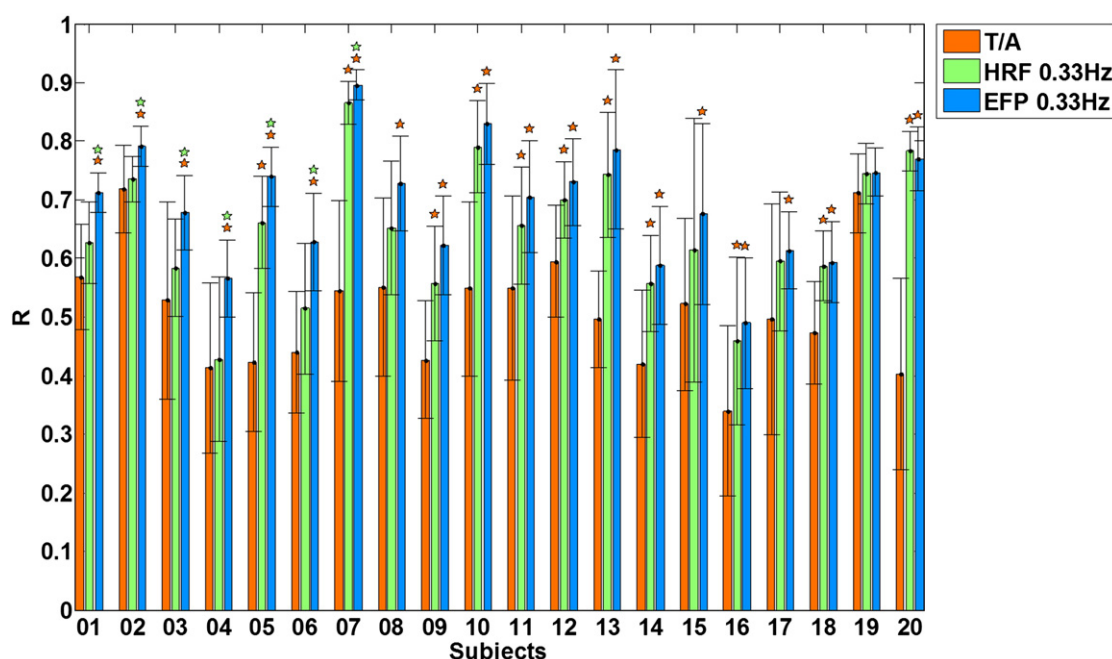


Fig. 6. Performance comparison between the T/A predictor, HRF and EFP predictors. Results of the EFP method indicate that 85% of the subjects achieved correlation higher than 0.6. In addition, EFP prediction improvement was obtained compared to T/A predictor, in all subjects (95% of them were significant). EFP prediction improvement was obtained with respect to the HRF predictor, in 90% of the subjects (35% of them were significant). The star's color represents the method that obtained significance (* $p < 0.05$). The subjects are ordered by an increasing p-value. The error bars are standard deviations over the cross-validation mk-folds. All methods were tested on the same train-test division.

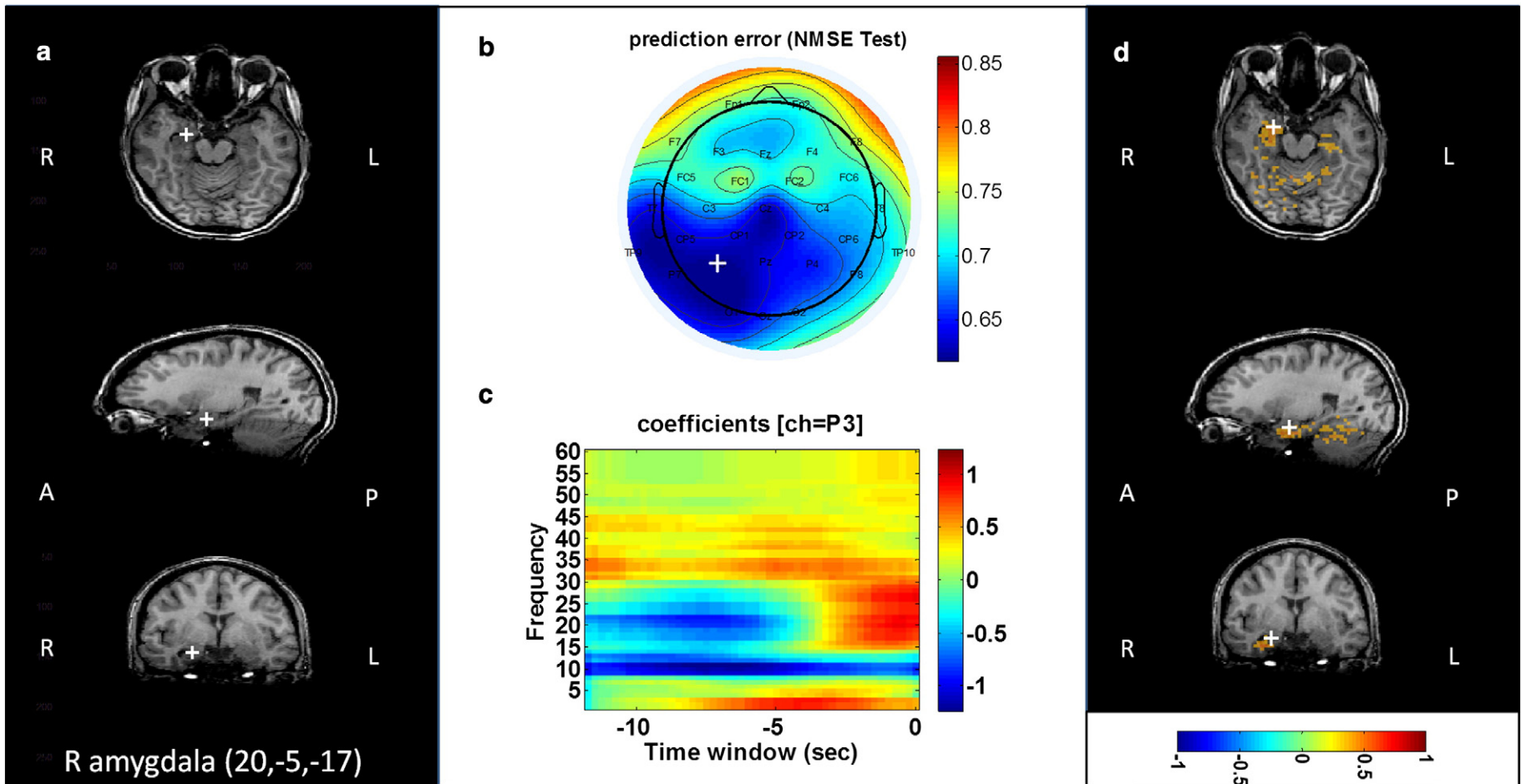


Fig. 7. The EFP for the amygdala. a) The target ROI extracted from the right amygdala (Talairach [20, -5, -17], MNI [20, -4, -21], Gaussian sphere radius 6 mm) b) Averaged prediction error (NMSE) on test data with the target ROI ($n = 17$, $p < 0.05$, FDR corrected) for each electrode for all the selected subjects (i.e. the subjects that achieved prediction correlation above 0.6 on validation sets). The colors depict that electrode P3 produced the minimal NMSE (i.e. best predict the activity in the right amygdala ROI). c) EFPs from electrode P3 averaged across all the selected subjects ($n = 17$, $p < 0.05$, FDR corrected). Activity modulation in the theta, alpha, beta and gamma frequency bands is clearly evident as correlating to the amygdala BOLD activity. It is important to note however that the delay between the signals in each modality differs between frequencies. d) Slices of the same section as in 7a, obtained from the whole brain parametric maps for all the selected subjects show the distribution of activated voxels that are strongly predicted by the EFP of electrode P3 ($|R| \geq 0.35$, $p < 0.05$, FDR corrected). The bottom bar shows the Pearson correlation value between signal intensity and EFP predictor.

based on the findings of Ben-Simon et al. (2008), Goldman et al. (2002), Moosmann et al. (2003), which showed that the alpha predictor is negatively correlated to the BOLD signal in this area. Our expectation was to reproduce those findings using the suggested algorithm.

The algorithm was applied separately for each subject. Prediction results (i.e. correlation to target fMRI signal) using the electrode that gave minimum NMSE on the validation sets, were compared to prediction results using alpha predictor (see section "Experiment setup and pre-processing") and to those, which use a linear combination of frequencies with a pre-defined delay instead of a variable-delay (i.e. HRF predictor). The pre-defined delay was obtained by convolving the original EEG time-frequency data with the canonical hemodynamic response function (HRF) implemented in SPM (inspired by Zumer et al., 2010).

Fig. 4 depicts results of comparison of the above methods when sampled at the original fMRI temporal resolution (to isolate the effect of up-sampling). Results indicate significant improvement of the EFP predictor compared to the Alpha predictor, in all subjects. EFP prediction improvement was obtained with respect to the HRF predictor in all of the subjects (75% of them were significant).

Fig. 5 summarizes results of our EFP approach for all 4 subjects. It shows the averaged prediction error (NMSE) on test data for each electrode over the entire group (**Fig. 5b**) and the averaged EFP for the electrode that gave minimum NMSE on the validation sets on average over all the subjects (**Fig. 5c**). The ridge coefficients for each subject were normalized before averaging. Results reinforce previous findings with eyes-closed-eyes-opened paradigms; during eyes closed, an increased alpha power can be observed in the occipital regions (known as the "Berger effect"). The negative coefficients in the alpha band stand for the known inverse relationship between alpha activity and the fMRI-blood-oxygen level-dependent (BOLD) signal in the occipital cortex (Moosmann et al., 2003). The coefficients further indicate that the delay between the modalities is around 3 s. To explicitly test the spatial specificity of the EFP found at electrode P3, we performed a whole brain parametric analysis on the fMRI data sets. **Fig. 5d** demonstrates the BOLD activations that are strongly predicted by this EFP on average over the entire set of subjects.

Prediction of subcortical/limbic activity

After the initial encouraging results on cortical regions, we have applied the suggested algorithm to a sub-cortical region such as the amygdala, which is a major node in a limbic network known to mediate the organism's emotional states and motivation, thus plays crucial role during stress response (LeDoux, 2000). The activity of the amygdala was obtained from a simultaneous recording of EEG/fMRI test in which participants were instructed to relax while receiving an auditory feedback guided on-line by their theta/alpha ratio modulation (see Kinreich et al., 2011b and method section for additional details). The decision to focus on the amygdala for the relaxation data was based on a previous work in our lab (Admon et al., 2009), which was performed on soldiers and showed that healthy individuals with heightened

amygdala reactivity are at a greater risk to exhibit more stress symptoms after exposure to real-life stressful events. This finding is reinforced in the review (Admon et al., 2013).

The EFP approach was applied on ROI extracted from the right amygdala (Talaraiach [20, -5, -17], MNI [20, -4, -21], Gaussian sphere radius 6 mm). The right amygdala was chosen based on previous findings indicating its reactivity to intense stress (Kinreich et al., 2011a) and its coordinates were based on the findings of a comprehensive meta-analysis of 162 emotion studies (Kober et al., 2008), classifying the amygdala as a member of a limbic cluster.

The algorithm was applied separately for each subject. Prediction results were compared to those based on Theta/Alpha predictor (see section "Experiment setup and pre-processing") and to those, which use a linear combination of frequencies with a pre-defined delay instead of a variable-delay (i.e. HRF predictor). The pre-defined delay was obtained by convolving the original EEG time-frequency data with the canonical hemodynamic response function (HRF) implemented in SPM (inspired by Zumer et al., 2010).

Fig. 6 depicts results of comparison of the above methods when sampled at the original fMRI temporal resolution (to isolate the effect of up-sampling). Results of the EFP method indicate that 85% of the subjects achieved correlation higher than 0.6. In addition, EFP prediction improvement was obtained compared to T/A predictor, in all subjects (95% of them were significant). EFP prediction improvement was obtained with respect to the HRF predictor in 90% of the subjects (35% of them were significant).

Fig. 7 summarizes results for all subjects that achieved correlation above 0.6 on validation data with the target ROI. The correlation threshold was selected to minimize the NMSE prediction error on the validation sets. There were 17 such subjects out of a pool of 20 subjects. The averaged prediction error (NMSE) on test data for each electrode over those subjects (**Fig. 7b**) and the averaged EFP for the electrode that gave minimum NMSE on the validation sets (**Fig. 7c**) are depicted. The coefficients for each subject were normalized before averaging. Results indicate that electrode P3 produced minimal NMSE (i.e. best describe the activity in the right amygdala) and the activated frequencies were theta, alpha, beta and gamma. To explicitly test the spatial specificity of the EFP found at electrode P3, we performed a whole brain parametric analysis on the fMRI data sets. **Fig. 7d** demonstrates the BOLD activations that are strongly predicted by this EFP on average over the above selected subjects. The results reinforce the specificity of the model and show that the right amygdala is strongly predicted by this EFP. The whole brain parametric analysis is demonstrated in (Inline Supplementary Fig. S3).

Inline Supplementary Fig. S3 can be found online at <http://dx.doi.org/10.1016/j.neuroimage.2013.11.004>.

Two important observations arise from the results; first the band limits were not uniform between subjects therefore, a uniform division into alpha-theta may not be appropriate for all the subjects. Second, we add to previous results (Aguirre et al., 1998) and show that the delay between the modalities differs between subjects, electrodes and frequencies. The varying delay between frequencies is illustrated in

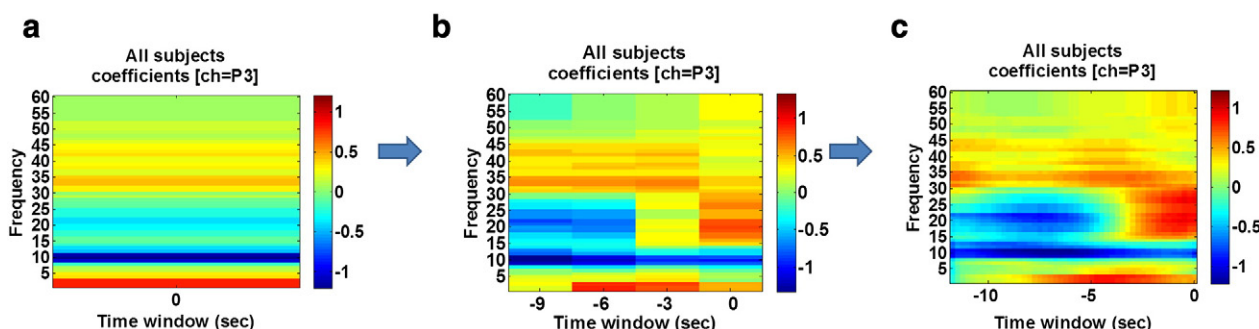


Fig. 8. The effect of the up-sampling on the averaged EFP for electrode P3 averaged for all the selected subjects (n = 17). a) HRF 0.33Hz b) EFP 0.33Hz c) EFP 4Hz.

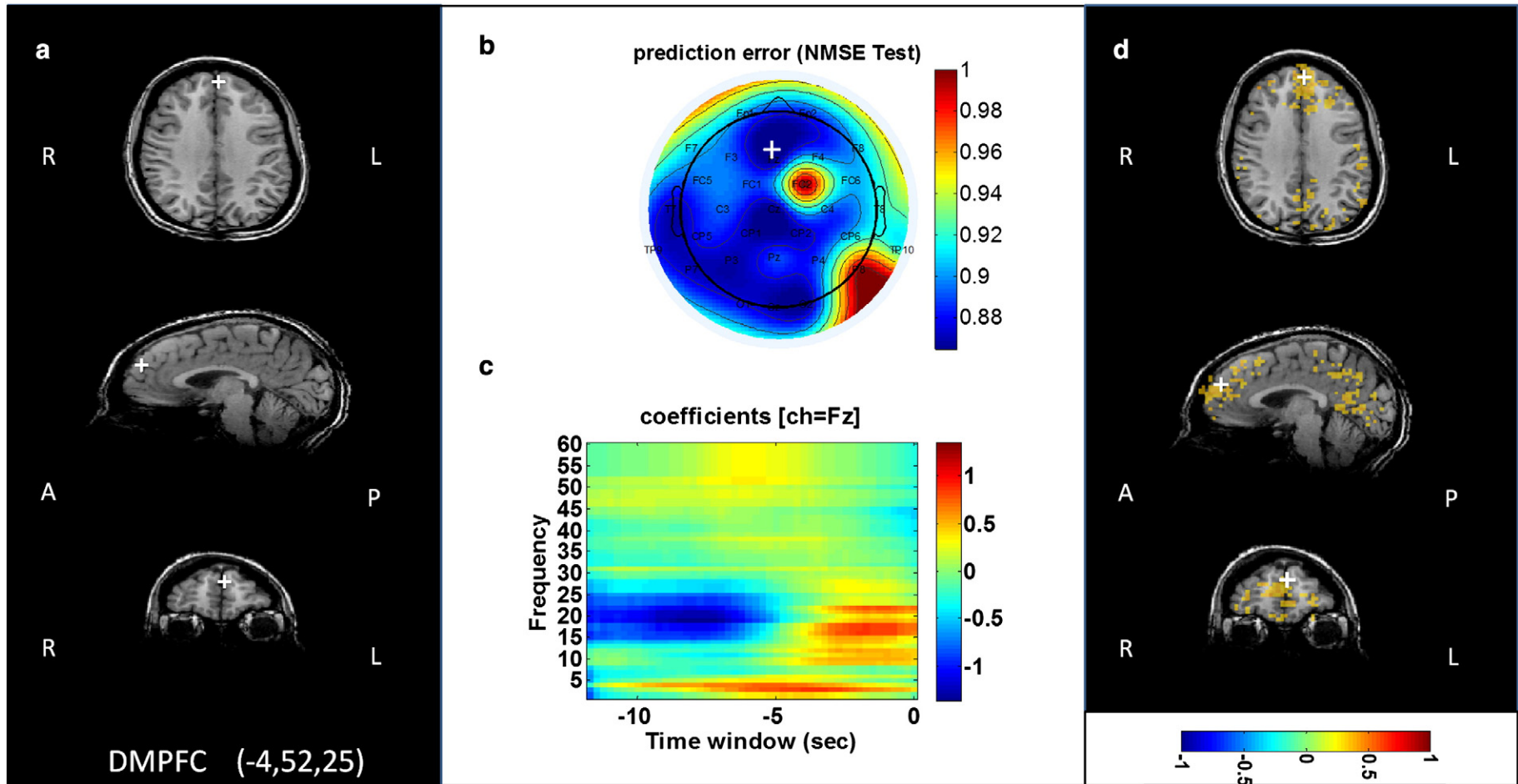


Fig. 9. The EFP for the dmPFC. a) The target ROI extracted from the dmPFC (Talairach [-4, 52, 25], MNI [-4, 52, 30], Gaussian sphere radius 6 mm) b) Averaged prediction error (NMSE) on test data with the target ROI ($n = 16$, $p < 0.05$, FDR corrected) for each electrode for all the selected subjects (i.e. the subjects that achieved prediction correlation above 0.4 on validation sets). Figure depicts that the electrode Fz produced the minimal NMSE (i.e. best describe the activity in the dmPFC ROI). c) Averaged EFP for electrode Fz of all those subjects ($n = 16$, $p < 0.05$, FDR corrected). The change in EEG activity in the theta, alpha and beta frequency bands is evident. Note that the EFP found for the dmPFC relative to the one found for the Amygdala, provides a different distribution over EEG electrodes and different distribution over frequencies and time-delays. d) Slices of the same section as in 9a, obtained from the whole brain parametric maps for all the selected subjects show the distribution of activated voxels that are strongly predicted by the EFP of electrode Fz ($|R| > 0.3$, $p < 0.05$, FDR corrected). The results show that the dmPFC is strongly predicted by this EFP along with other regions in the medial wall. The bottom bar shows the Pearson correlation value between signal intensity and EFP predictor.

electrode P3; the peak of the alpha and the beta bands precede the peak of the theta band. Inline Supplementary Fig. S4 demonstrates the varying delay between subjects and the varying delay between electrodes.

Inline Supplementary Fig. S4 can be found online at <http://dx.doi.org/10.1016/j.neuroimage.2013.11.004>.

The EFP method predicts the fMRI BOLD signal from the EEG. It assumes that both signals have the same temporal resolution. The temporal resolution of the signals can be as low as the fMRI temporal resolution or have a higher temporal resolution (by reducing the EEG temporal resolution and up-sampling the temporal resolution of the fMRI signal). No evidence was found to prediction correlation improvement due to the up-sampling. However, higher temporal resolution of the fMRI signal and higher temporal resolution of the EEG respectively, may shed light on brain processes as can be seen from Fig. 8; increasing the signals' resolution is reflected in the smoothness of the EFP coefficients.

The proposed framework for constructing EFP utilizes machine learning and signal processing methods to create a robust EEG model of fMRI deep brain activation. Ridge regression was used to demonstrate it, but it can be applied also with variety of linear and non-linear regressors. One additional example can be using regularized least squares (LASSO) (Kim et al., 2007; Tibshirani, 1996). Comparison to Lasso (see Inline Supplementary Fig. S5) indicates that Ridge prediction results are slightly better than Lasso (in 85% of the subjects, 20% of them are significant).

Inline Supplementary Fig. S5 can be found online at <http://dx.doi.org/10.1016/j.neuroimage.2013.11.004>.

To test whether the findings are specific to the amygdala or to the paradigm, the method was applied to additional region that is known to be involved in stress regulation; the mPFC area (Shin et al., 2005). The specific ROI was extracted from the mPFC (Talaraiach [-4, 52, 25], MNI [-4, 52, 30], Gaussian sphere radius 6 mm). The dmPFC coordinates (as the amygdala coordinates), were based on the findings of a comprehensive meta-analysis of 162 emotion studies (Kober et al., 2008), classifying the dmPFC as a member of emotional regulation network.

Fig. 9 summarizes results for all subjects that achieved correlation above 0.4 on validation data with the target ROI. The correlation threshold was selected to minimize the NMSE prediction error on the validation sets. There were 16 such subjects out of a pool of 20 subjects. The averaged prediction error (NMSE) on test data for each electrode over those subjects (Fig. 9b) and the averaged EFP for the electrode that gave minimum NMSE on the validation sets (Fig. 9c) are depicted. The coefficients for each subject were normalized before averaging. Results indicate that electrode Fz produced minimal NMSE (i.e. best describe the activity in the dmPFC) and the activated frequencies were theta, alpha and beta. To explicitly test the spatial specificity of the EFP found at electrode Fz, we performed a whole brain parametric analysis on the fMRI data sets. Fig. 9d demonstrates the BOLD activations that are strongly predicted by this EFP on average over the above selected subjects. The results reinforce the specificity of the additional EFP model and show that the dmPFC is strongly predicted by it. The whole brain parametric analysis is demonstrated in (see Inline Supplementary Fig. S6).

Inline Supplementary Fig. S6 can be found online at <http://dx.doi.org/10.1016/j.neuroimage.2013.11.004>.

Two important observations arise from this analysis when comparing the EFP developed for the amygdala and the one for the dmPFC; first, the EFPs provide two different distributions over the scalp; while the amygdala was best predicted by electrode P3, the mPFC was best predicted by electrode Fz. Second, the EFPs provide two different frequency patterns; relative to the amygdala's EFP, in the dmPFC's EFP gamma band is not contributing and the alpha has weaker and opposite behavior with an earlier delay.

Discussion

We introduced a framework for constructing EEG Finger-Print (EFP) derived from fMRI deep region activity. The framework utilizes machine

learning and signal processing methods to create a robust EEG model from a single electrode. This robust EEG model senses a signal that is correlated with the BOLD signal that describes or has been highly correlated with the activity in deep brain regions. It therefore, may reduce the need for fMRI in the context of brain guided training or diagnostics in psychiatry and neurology.

The brain activity from a region of interest was modeled using a linear combination of frequencies where each frequency band has its own delay. Specifically, an optimization function which searches in the full matrix of the time/frequency representation was applied rather than searching in the vector of frequency representation (Zumer et al., 2010) or searching a specific HRF for each frequency separately (de Munck et al., 2007, 2009). Moreover, no constraints were imposed on the HRF but instead the generalized HRF was optimized from the full time/frequency representation of the EEG signal. Results using this methodology support previous findings that the hemodynamic response function differs between subjects, electrodes and frequencies (Aguirre et al., 1998) and show that individual brain activity as measured by the fMRI BOLD signal in deep brain regions can be better predicted using different time-delays for different frequencies without making any assumption on the HRF shape.

The suggested framework maintains high frequency EEG information, by sub-sampling the spectral power rather than the raw signal. Often, integration of EEG and fMRI requires down-sampling of the EEG signal or convolution with low frequency signal (such as the HRF) to match the fMRI resolution. Reducing the temporal resolution of the EEG may ignore important temporal information stored in the EEG that might be important to understand the brain activity. Reducing the temporal resolution (sampling) of the spectral power of the EEG signal (i.e. reducing the sampling of the power in different frequencies) as was done in De Martino et al. (2010), instead of reducing the sampling of the EEG raw signal, will reduce the loss of information since the changes in the spectral power of the EEG signals are slower than the original ones (Stockwell, 2007). Moreover, the temporal resolution of the spectral power of the EEG was slightly reduced and in parallel the temporal resolution of the BOLD signal was slightly increased, to reduce the loss of information. This approach was reflected in the smoothness of the EFP coefficients.

The EFP, created using the suggested framework may suggest three observations on the EEG brain activity related to the selected fMRI targets: First, it shows that the theta, alpha, beta and gamma frequency bands contribute all together to the prediction of fMRI BOLD signal modulation in the target regions (i.e. amygdala or dmPFC). This finding is consistent with prior studies that investigated the EEG spectral power during relaxation and found those frequency bands (occipital-alpha, beta and theta) as informative measures for relaxation (Chen et al., 2008; Jacobs and Friedman, 2004; Jacobs and Lubar, 1989; Jacobs et al., 1996; Lee et al., 2012).

Second, our EFP pattern may indicate differential change of the power spectrum depending on the fMRI origin of the EFP; during a gradual attempt to relax, results indicate that activity of the amygdala is correlated with increased power modulation of theta but decreased modulation of alpha. These results reinforce the finding that as individual becomes drowsier the dominant frequency commonly shifts from faster frequency to slower frequency bands (Vogel et al., 1966). In contrast, activity of the dmPFC correlated with increased theta as well as alpha modulations. Altogether the unique patterns of band modulations per EFP, may point to the different roles of the amygdala and dmPFC for inducing relaxation. Indeed it was previously shown that frontal and limbic areas exhibited distinctly different activity patterns during the transition into relaxation (e.g. hippocampus and Middle frontal G) (Picchioni et al., 2008).

Third, the best correlation with the amygdala was obtained with a different electrode and different weights of frequencies and time-delays than the best correlation with the dmPFC. This indicates that the amygdala and the dmPFC may derive different type and origin of

electrical activity. This is clearly evident by the fact that each EFP target revealed strikingly different correlation maps; the amygdala derived EFP was correlated with a limbic/perceptual network more involved in bottom-up/local processing of information related to simple forms of affective perception, learning, and memory encoding. In contrast the EFP derived from the dmPFC was correlated with a network involved in top-down control processing that is based on cognitive attribution and interpretations (Ochsner et al., 2009).

One may argue that these EFP characteristics have resulted from the paradigm and not from the changes of activity of the amygdala. To test this claim, the EFP created using the suggested framework for the amygdala need to be validated in a context different than relaxation. Moreover, although we predicted the BOLD activity in the amygdala, it is also possible that the resulted EFP actually represents the cortical network and not the amygdala's activity itself and in this case, the different delays may be due to different cortical generators.

The framework does not assume a-priori knowledge on the experiment or on the activated electrodes and frequencies but applied a data-driven approach to divide the frequency range into frequency bands and to find the most relevant electrodes and frequencies which contribute the most to the fMRI ROI prediction. This allows us to apply this framework on any experiment, in particular involving deep brain activity. In addition, the use of a machine learning approach combined with robust statistic for model selection and validation, resulted in a model which is capable to predict unseen fMRI BOLD signal. Currently, EFP finds an individual model for each subject, but our ultimate goal is to extract a common model, which overcomes the differences between subjects and suggests a tool to predict the ROI for subjects which did not participated in model construction. Preliminary results indicate that prediction difference between a model suitable for several subjects and individual models are minor.

This research may have practical implementations in neuroscience as well as medicine for brain guided monitoring, diagnosis and intervention (e.g. neuro-feedback). Improving the spatial resolution of the EEG, may result in obtaining sufficient information on sub-cortical regions using EEG only, to better understand neural mechanisms of critical behavioral control mechanism such as emotion regulation, learning acquisition and action planning. Furthermore, this can provide an improved region-specific basis for closed-loop EEG procedures for a various neuro-feedback tasks.

Acknowledgments

We would like to thank all those who contributed in this research in The Wohl Institute for Advanced Imaging at the Tel Aviv Sourasky Medical Center and in particular to Eti Ben-Simon for helping to collect and analyze the data and Shahar Jamshy for his comments and insights. This study was supported by grants from the U.S. Department of Defense award number W81XWH-11-2-0008, the Adams Super Center for Brain Studies and the Israeli Scientific Foundation converging technologies program.

Appendix A. Supplementary data

Supplementary data to this article can be found online at <http://dx.doi.org/10.1016/j.neuroimage.2013.11.004>.

References

- Ackermans, L., Temel, Y., Visser-Vandewalle, V., 2008. Deep brain stimulation in Tourette's syndrome. *Neurotherapeutics* 5, 339–344.
- Admon, R., Lubin, G., Stern, O., Rosenberg, K., Sela, L., Ben-Ami, H., Hendler, T., 2009. Human vulnerability to stress depends on amygdala's predisposition and hippocampal plasticity. *PNAS* 106 (33), 14120–14125.
- Admon, R., Mriad, M.R., Hendler, T., 2013. A causal model of post-traumatic stress disorder: disentangling predisposed from acquired neural abnormalities. *Trends Cogn. Sci.* 17 (7), 337–347.
- Adolphs, R., Tranel, D., Damasio, H., Damasio, A., 1995. Fear and the human amygdala. *J. Neurosci.* 15 (9), 5879–5891.
- Aguirre, G.K., Zarahn, E., D'Esposito, M., 1998. The variability of human, BOLD hemodynamic responses. *NeuroImage* 8 (4), 360–369.
- Ahlfors, S.P., Simpson, G.V., 2004. Geometrical interpretation of fMRI-guided MEG/EEG inverse estimates. *NeuroImage* 22 (1), 323–332.
- Ahlfors, S.P., Simpson, G.V., Dale, A.M., Belliveau, J.W., Liu, A.K., Korvenoja, A., Virtanen, J., Huotilainen, M., Tootell, R.B.H., Aronen, H.J., Ilmoniemi, R.J., 1999. Spatiotemporal activity of a cortical network for processing visual motion revealed by MEG and fMRI. *Neurophysiology* 82, 2545–2555.
- Atick, J.J., Redlich, A., 1992. What does the retina know about natural scenes. *Neural Comput.* 4, 196–211.
- Babiloni, F., Cincotti, F., Babiloni, C., Carducci, F., Basilisco, A., Rossini, P.M., Mattia, D., Astolfi, L., Ding, L., Ni, Y., Cheng, K., Christine, K., Sweeney, J., He, B., 2005. Estimation of the cortical functional connectivity with the multimodal integration of high resolution EEG and fMRI data by directed transfer function. *NeuroImage* 24, 118–131.
- Baillet, S., Mosher, J., Leahy, R., 2001. Electromagnetic brain mapping. *IEEE Signal Process.* 14–30.
- Ben-Simon, E., Podlipsky, I., Arieli, A., Zhdanov, A., Hendler, T., 2008. Never resting brain: simultaneous representation of two alpha related processes in humans. *PLoS One* 3 (12), e3984.
- Bießmann, F., Meinecke, F.C., Gretton, A., Rauch, A., Rainer, G., Logothetis, N.K., Müller, K.-R., 2010. Temporal kernel CCA and its application in multimodal neuronal data analysis. *Mach. Learn.* 79, 5–27.
- Brookings, T., Ortigue, S., Grafton, S., Carlson, J., 2009. Using ICA and realistic BOLD models to obtain joint EEG/fMRI solutions to the problem of source localization. *NeuroImage* 44, 411–420.
- Calhoun, V.D., Adali, T., 2009. Feature-based fusion of medical imaging data. *IEEE Trans. Inf. Technol. Biomed.* 13 (5), 711–720.
- Chen, L.L., Sugi, T., Shirakawa, S., Zou, J.Z., Nakamura, M., 2008. Systematic evaluation of relaxation circumstances based on bio-neurological signals. *Proceedings of the 17th World Congress The International Federation of Automatic Control, Seoul, Korea.*
- Correa, N.M., Eichele, T., Adali, T., Li, Y.-O., Calhoun, V.D., 2010. Multi-set canonical correlation analysis for the fusion of concurrent single trial ERP and functional MRI. *NeuroImage* 50 (4), 1438–1445.
- Dale, A.M., Liu, A.K., Fischl, B.R., Buckner, R.L., Belliveau, J.W., Lewine, J.D., Halgren, E., 2000. Dynamic statistical parametric mapping: combining fMRI and MEG for high-resolution imaging of cortical activity. *Neuron* 26, 55–67.
- Daunizeau, J., Grova, C., Marrelec, G., Mattout, J., Jbabdi, S., Pelegri-Issac, M., Lina, J.M., Benali, H., 2007. Symmetrical event-related EEG/fMRI information fusion in a variational Bayesian framework. *NeuroImage* 36 (1), 69–87.
- De Martino, F., de Bort, A.W., Valente, G., Goebel, R., Formisano, E., 2010. Predicting EEG single trial responses with simultaneous fMRI and relevance vector machine regression. *NeuroImage* 56 (2), 826–836.
- de Munck, J.C., Gonçalves, S.I., Huijboom, L., Kuijper, J.P., Pouwels, P.J., Heethaar, R.M., Lupe da Silva, F.H., 2007. The haemodynamic response of the alpha rhythm: an EEG/fMRI study. *NeuroImage* 35 (3), 1142–1151.
- de Munck, J.C., Gonçalves, S.I., Mammoliti, R., Heethaar, R.M., Lopes da Silva, F.H., 2009. Interactions between different EEG frequency bands and their effect on alpha-fMRI correlations. *NeuroImage* 47, 69–76.
- Debener, S., Ullsperger, M., Siegel, M., Fiehler, K., Yves von Cramon, D., Engel, A.K., 2005. Trial-by-trial coupling of concurrent electroencephalogram and functional magnetic resonance imaging identifies the dynamics of performance monitoring. *J. Neurosci.* 25 (50), 11730–11737.
- Deneux, T., Faugeras, O., 2010. EEG-fMRI fusion of paradigm-free activity using Kalman filtering. *Neural Comput.* 22, 906–948.
- Efron, B., Tibshirani, R., 1993. *An Introduction to the Bootstrap*, 57th edition. CRC.
- Egner, T., Strawson, E., Grzelcier, J.H., 2002. EEG signature and phenomenology of alpha/theta neurofeedback training versus mock feedback. *Appl. Psychophysiol. Biofeedback* 27 (4), 261–270.
- Eichele, T., Specht, K., Moosmann, M., Jongsma, M.L.A., Quian Quiroga, R., Nordby, H., Hugdahl, K., 2005. Assessing the spatiotemporal evolution of neuronal activation with single-trial event-related potentials and functional MRI. *PNAS* 102 (49), 17798–17803.
- Friston, K.J., Jezzard, P., Turner, R., 1994. Analysis of functional MRI time-series. *Hum. Brain Mapp.* 1, 153–171.
- Genger, N.G., Acar, C.E., 2004. Sensitivity of EEG and MEG measurements to tissue conductivity. *Phys. Med. Biol.* 49, 701–717.
- Goldman, R.I., Stern, J.M., Engel Jr, Cohen, M., 2002. Simultaneous EEG and fMRI of the alpha rhythm. *NeuroReport* 13 (18), 2487–2492.
- Gonçalves, S.I., de Munck, J.C., Pouwels, P.J.W., Schoonhoven, R., Kuijper, J.P.A., Maurits, N.M., Hoogduin, J.M., Van Someren, E.J.W., Heethaar, R.M., da Silva, F.H.L., 2006. Correlating the alpha rhythm to BOLD using simultaneous EEG/fMRI: inter-subject variability. *NeuroImage* 30 (1), 203–213.
- Grech, R., Cassar, T., Muscat, J., Camilleri, K.P., 2008. Review on solving the inverse problem in EEG source analysis. *J. Neuroeng. Rehabil.* 5 (25).
- Haraldsson, H.M., Ferrarelli, F., Kalin, N.H., Tononi, G., 2004. Transcranial magnetic stimulation in the investigation and treatment of schizophrenia: a review. *Schizophr. Res.* 71, 1–16.
- Harris-Warrick, R., Marder, E., 1991. Modulation of neural networks for behavior. *Annu. Rev. Neurosci.* 14, 39–57.
- Hasson-Meir, Y., Zhdanov, A., Hendler, T., Intrator, N., 2011. Inference of brain mental states from spatio-temporal analysis of EEG single trials. *Proceedings of the international conference on bio-inspired systems and signal processing*, pp. 59–66.
- Henson, R.N., Flandin, G., Friston, K.J., Mattout, J., 2010. A parametric empirical Bayesian framework for fMRI-constrained MEG/EEG source reconstruction. *Hum. Brain Mapp.* 31 (10), 1512–1531.

- Hoerl, A.E., Kennard, R.W., 1970. Ridge regression: biased estimation for nonorthogonal problems. *Technometrics* 12 (1), 55–67.
- Honey, C.R., Ranjan, M., 2012. Deep brain stimulation for Parkinson's disease – a review. *Eur. Neurol. Rev.* 7 (1), 28–34.
- Horowitz, S., 2012. Neurofeedback therapy in clinical applications and for cognitive enhancement. *Alternat. Complement. Ther.* 18 (5), 242–247.
- Huster, R.J., Debener, S., Eichele, T., Herrmann, C.S., 2012. Methods for simultaneous EEG-fMRI: an introductory review. *J. Neurosci.* 32 (18), 6053–6060.
- Jacobs, G.D., Friedman, R., 2004. EEG spectral analysis of relaxation techniques. *Appl. Psychophysiol. Biofeedback* 29 (4).
- Jacobs, G.D., Lubar, J.F., 1989. Spectral analysis of the central nervous system effects of the relaxation response elicited by autogenic training. *Behav. Med.* 15 (3), 125–132.
- Jacobs, G., Benson, H., Friedman, R., 1996. Topographic EEG mapping of the relaxation response. *Biofeedback Self Regul.* 21 (2), 121–129.
- Kim, S.-J., Koh, K., Lustig, M., Boyd, S., Gorinevsky, D., 2007. An interior point method for large-scale 11-regularized least squares. *J-STSP* 1, 606–617.
- Kinreich, S., Intrator, N., Hendler, T., 2011a. Functional cliques in the amygdala and related brain networks driven by fear assessment acquired during movie viewing. *Brain Connect.* 1 (6), 484–495.
- Kinreich, S., Podlipsky, I., Intrator, N., Hendler, T., 2011b. Categorized EEG neurofeedback performance unveils simultaneous fMRI deep brain activation. Proceedings of NIPS Workshop on Machine Learning and Interpretation in Neuroimaging. Springer LNAI State-of-the-art Survey, vol. 7263.
- Kober, H., Feldman Barrett, L., Joseph, J., Eliza, B.-M., Lindquist, K., Wager, T.D., 2008. Functional grouping and cortical–subcortical interactions in emotion: a meta-analysis of neuroimaging studies. *NeuroImage* 42, 998–1031.
- Korvenoja, A., Huttunen, J., Salli, E., Pohjonen, H., Martinkauppi, S., Palva, J.M., Lauronen, L., Virtanen, J., Ilmoniemi, R.J., Aronen, H.J., 1999. Activation of multiple cortical areas in response to somatosensory stimulation: combined magnetoencephalographic and functional magnetic resonance imaging. *Hum. Brain Mapp.* 8, 13–27.
- Lang, P., Davis, M., Öhman, A., 2000. Fear and anxiety: animal models and human cognitive psychophysiology. *J. Affect. Disord.* 61 (3), 137–159.
- Lauks, H., Kleinschmidt, A., Beyerle, A., Eger, E., Salek-Haddadi, A., Preibisch, C., Krakow, K., 2003a. EEG-correlated fMRI of human alpha activity. *NeuroImage* 40 (19), 1463–1476.
- Lauks, H., Krakow, K., Sterzer, P., Eger, E., Beyerle, A., Salek-Haddadi, A., Kleinschmidt, A., 2003b. Electroencephalographic signatures of attentional and cognitive default modes in spontaneous brain fluctuations at rest. *PNAS* 100 (19), 11053–11058.
- LeDoux, J., 1992. In: Aggleton, J.P. (Ed.), *Emotion and the Amygdala*. Wiley-Liss, New York.
- LeDoux, J.E., 2000. Emotion circuits in the brain. *Annu. Rev. Neurosci.* 23, 155–184.
- Lee, E.-J., Bhattacharya, J., Sohn, C., Verres, R., 2012. Monochord sounds and progressive muscle relaxation reduce anxiety and improve relaxation during chemotherapy: a pilot EEG study. *Complement. Ther. Med.* 20, 409–416.
- Liu, Z., He, B., 2008. fMRI-EEG integrated cortical source imaging by use of time-variant spatial constraints. *NeuroImage* 39, 1198–1214.
- Liu, A.K., Belliveau, J.W., Dale, A.M., 1998. Spatiotemporal imaging of human brain activity using functional MRI constrained magnetoencephalography data: Monte Carlo simulations. *Proc. Natl. Acad. Sci.* 95 (15), 8945–8950.
- Liu, Z., Kecman, F., He, B., 2006. Effects of fMRI-EEG mismatches in cortical current density estimation using fMRI and EEG: a simulation study. *Clin. Neurophysiol.* 117, 1610–1622.
- Luessi, M., Babacan, S., Molina, R., Booth, J., Katsaggelos, A., 2011. Bayesian symmetrical EEG/fMRI fusion with spatially adaptive priors. *NeuroImage* 55, 113–132.
- Martinez-Montes, E., Valdes-Sosa, P.A., Miwakeichi, F., Goldman, R.I., Cohen, M.S., 2004. Concurrent EEG/fMRI analysis by multiway partial least squares. *NeuroImage* 22, 1023–1034.
- Mattout, J., Phillips, C., Penny, W.D., Rugg, M.D., Friston, K.J., 2006. MEG source localization under multiple constraints: an extended Bayesian framework. *NeuroImage* 30, 753–767.
- Mink, J.W., 1996. The basal ganglia: focused selection and inhibition of competing motor programs. *Prog. Neurobiol.* 50, 381–425.
- Moosmann, M., Ritter, P., Krastel, I., Brink, A., Thees, S., Blankenburg, F., Taskin, B., Obrig, H., Villringer, A., 2003. Correlates of alpha rhythm in functional magnetic resonance imaging and near infrared spectroscopy. *NeuroImage* 20 (1), 145–158.
- Moosmann, M., Eichele, T., Nordby, H., Hugdahl, K., Calhoun, V.D., 2008. Joint independent component analysis for simultaneous EEG-fMRI: principle and simulation. *Int. J. Psychophysiol.* 67, 212–221.
- Novakovic, V., Sher, L., Lapidus, K.A.B., Mindes, J., Golier, J.A., Yehuda, R., 2011. Brain stimulation in posttraumatic stress disorder. *Eur. J. Psychotraumatol.* 2.
- Ochsner, K.N., Ray, R.R., Hughes, B., McRae, K., Cooper, J.C., Weber, J., Gabrieli, J.D.E., Gross, J.J., 2009. Bottom-up and top-down processes in emotion generation: common and distinct neural mechanisms. *Physiol. Sci.* 20 (11), 1322–1331.
- Ou, W., Nummenmaa, A., Ahveninen, J., Belliveau, J.W., Härmäläinen, M.S., Golland, P., 2010. Multimodal functional imaging using fMRI-informed regional EEG/MEG source estimation. *NeuroImage* 52 (1), 97–108.
- Pandurangi, A.K., Fernicola-Bledowski, C., Bledowski, J., 2012. Brain stimulation therapies for psychiatric disorders: the first decade of the new millennium – a review. *Asian J. Psychiatry* 5 (1), 3–10.
- Peniston, E.G., Kulkosky, P.J., 1991. Alpha-theta brainwave neurofeedback for Vietnam veterans with combat-related post-traumatic stress disorder. *Med. Psychother.* 4 (1), 47–60.
- Phillips, C., Rugg, M.D., Friston, K.J., 2002. Anatomically informed basis functions for EEG source localization: combining functional and anatomical constraints. *NeuroImage* 16 (3 Pt 1), 678–695.
- Phillips, C., Mattout, J., Rugg, M.D., Maquet, P., Friston, K.J., 2005. An empirical Bayesian solution to the source reconstruction problem in EEG. *NeuroImage* 24, 997–1011.
- Picchioni, D., Fukunaga, M., Carr, W.S., Braun, A.R., Balkin, T.J., Duyn, J.H., Horovitz, S.G., 2008. fMRI differences between early and late stage-1 sleep. *Neurosci. Lett.* 441 (1), 81–85.
- Podlipsky, I., Ben-Simon, E., Hendler, T., Intrator, N., 2012. Robust modeling based on optimized EEG bands for functional brain state inference. *J. Neurosci. Methods* 203, 377–385.
- Rauch, S., Shin, L., Phelps, E., 2006. Neurocircuitry models of posttraumatic stress disorder and extinction: human neuroimaging research – past, present, and future. *Biol. Psychiatry* 60 (4), 376–382.
- Rosa, M.J., Daunizeau, J., Friston, K.J., 2010. EEG-fMRI Integration: a critical review of biophysical modeling and data analysis approaches. *J. Integr. Neurosci.* 9 (4), 453–476.
- Sato, M.-a., Yoshioka, T., Kajihara, S., Toyama, K., Goda, N., Doya, K., Kawato, M., 2004. Hierarchical Bayesian estimation for MEG inverse problem. *NeuroImage* 23, 806–826.
- Shin, L.M., Wright, C.I., Cannistraro, P.A., Wedig, M.M., McMullin, K., Martis, B., Macklin, M.L., Lasko, N.B., Canavan, S.R., Krangel, T.S., Orr, S.P., Pitman, R.K., Whalen, P.J., Rauch, S.L., 2005. A functional magnetic resonance imaging study of amygdala and medial prefrontal cortex responses to overtly presented fearful faces in posttraumatic stress disorder. *Arch. Gen. Psychiatry* 62 (3), 273–281.
- Squire, L., 1992. Memory and the hippocampus: a synthesis from findings with rats, monkeys, and humans. *Psychol. Rev.* 9, 195–215.
- Stockwell, R.G., 2007. Why use the S-transform? *Fields Inst. Commun.* Ser. 52, 279–309.
- Stockwell, R.G., Mansinha, L., Lowe, R.P., 1996. Localization of the complex spectrum: the S transform. *IEEE Trans. Signal Process.* 44 (4), 998–1001.
- Storey, J.D., 2002. A direct approach to false discovery rates. *J. R. Stat. Soc. Ser. B Stat. Methodol.* 64 (3), 479–498.
- Tibshirani, R., 1996. Regression shrinkage and selection via the lasso. *J. R. Stat. Soc. Ser. B Stat. Methodol.* 267–288.
- Tikhonov, A., 1963. Solution of incorrectly formulated problems and the regularization method. *Sov. Math. Dokl.* 4, 1035–1038.
- Valdes-Sosa, P.A., Sanchez-Bornot, J.M., Sotero, R.C., Iturria-Medina, Y., Aleman-Gomez, Y., Bosch-Bayard, J., Carbonell, F., Ozaki, T., 2009. Model driven EEG/fMRI fusion of brain oscillations. *Hum. Brain Mapp.* 30, 2701–2721.
- Vogel, G., Foulkes, D., Trosman, H., 1966. Ego functions and dreaming during sleep onset. *Arch. Gen. Psychiatry* 14 (3), 238–248.
- Zald, D., 2003. The human amygdala and the emotional evaluation of sensory stimuli. *Brain Res. Rev.* 41 (1), 88–123.
- Zumer, J.M., Brookes, M.J., Stevenson, C.M., Francis, S.T., Morris, P.G., 2010. Relating BOLD fMRI and neural oscillations through convolution and optimal linear weighting. *NeuroImage* 49 (2), 1479–1489.